Journal of Nuclear Materials 390–391 (2009) 760–763

Contents lists available at ScienceDirect

Journal of Nuclear Materials

journal homepage: www.elsevier.com/locate/jnucmat

On the asymmetries of ELM divertor power deposition in JET and ASDEX Upgrade

T. Eich [a,*], A. Kallenbach [a], W. Fundamenski [b], A. Herrmann [a], V. Naulin [c], JET-EFDA contributors [1], ASDEX Upgrade team

[a] Max-Planck-Institut für Plasmaphysik, EURATOM-Association, Boltzmannstr. 2, D-85748 Garching, Germany
[b] EURATOM/UKAEA Fusion Association, Culham Science Centre, Abingdon, Oxon OX14 3DB, UK
[c] Association EURATOM–Risoe, DTU, P.O. Box 49, DK-4000 Roskilde, Denmark

ARTICLE INFO

PACS:
52.20.–j
52.25.Vy
52.30.Ex
52.55.Rk
52.55.Fa

ABSTRACT

An analytical expression was derived for describing the divertor target power during ELMs based on the model discussed in [W. Fundamenski, R.A. Pitts, Plasma Phys. Control. Fus. 48 (2006) 109] where the power load arises from a Maxwellian distribution of particles released into the SOL region. The paper discusses a comparable simple extension of the model by introducing a non-zero characteristic velocity of the Maxwellian distributed particles. This way the experimentally observed temporal evolution as well as the in/out energy imbalance can be described. The extended model named free-streaming-particle (FSP) approach predicts a dependence of the ELM in/out energy balance of the pedestal Mach number as well as an inversion of the in/out balance by a change of the field line helicity as observed experimentally. From the FSP approach the value for $E_{\tau_{IR}}$ (see text) is predicted to be 18–25% in good agreement to the experimental data. A comparison to the various discussed mechanism for the ELM in/out asymmetry is presented.

1. Introduction

H-mode plasmas develop a pronounced edge transport barrier and steep edge gradients driving quasi-periodic barrier relaxations known as edge localised modes (ELMs). Type-I ELMs impose a sudden release of energy from the pedestal region, from which the largest fraction is transported along field lines to the divertor region. Scaling of ELM losses and heat load from present devices show that the divertor life time in ITER will be limited due to ELMs [2–5].

Although good progress was achieved in recent years for ELM characterisation, still the observation of the larger fraction to be deposited on the inboard divertor with $-B_{tor}/+I_p$ (normal, i.e. ion $\nabla B \times B$ drift towards active X-point) field direction in lower-single null (LSN) magnetic configuration in JET, ASDEX Upgrade and DIII-D is not understood. For ASDEX Upgrade discharges in upper single null (USN) geometry with reversed field the larger fraction of ELM energy load is deposited on the outer divertor, whereas with normal field the larger fraction is on the inboard side, consistent to the LSN findings concerning the field direction dependent drifts but also the field line helicity. For the USN experiments in ASDEX Upgrade it also has been shown that charge separation takes place causing an excess amount of positive charges on the target side receiving the larger ELM energy load and roughly the same amount of negative charges on the other target [6]. The latter observation led to the conclusion that thermoelectric currents cannot explain the observed charge asymmetry, since the higher power load is observed at the cold electron side of the SOL.

Various explanations have been proposed to explain the observed in/out asymmetries which are briefly mentioned here. An increase of the sheath potential at the cold electron side due to a change of the edge current distribution during an ELM locally accelerating ions locally in front of the target plates was discussed for ASDEX Upgrade. However, this picture would require much larger increase of the potential than it was measured by Langmuir Probes [7]. For DIII-D data it was proposed that local conditions of the pre-ELM plasma in front of the targets plates play an important role. It was concluded that the colder divertor leg (commonly the inner leg for normal field direction) receives more ELM power due to a larger number of (cold) ions available for energy transport over the sheath. There, it was pointed out in particular that for high density discharges in DIII-D with small ELMs the larger fraction of ELM power is deposited on the inboard divertor [8]. Thirdly, direct ion orbit losses from the pedestal region during the ELM are predicted to preferentially hit the inner target plate in normal field and the outer target plate in reversed field if the typical ion energy is below the potential hill associated with the radial electric field commonly observed in H-mode plasmas [9]. However, from the latter model it is difficult to understand that in double-null discharges, as shown for DIII-D [10] and ASDEX Upgrade [11], literally no ELM power is deposited on the inboard targets.

* Corresponding author.
E-mail address: thomas.eich@ipp.mpg.de (T. Eich).

[1] See M.L. Watkins et al., Fusion Energy 2006 (Proceedings of the 21st International Conference Chengdu, 2006), IAEA, 2006.

0022-3115/$ - see front matter © 2009 Elsevier B.V. All rights reserved.
doi:10.1016/j.jnucmat.2009.01.202

This paper presents a possible contribution to the ELM power load asymmetry by taking into account the pedestal plasma rotation. We present experimental analysis of the temporal power evolution and time integrated energy values on the inner/outer target plates with both toroidal magnetic field directions ($\pm B_{tor}/+I_p$) and hence with both field line helicity orientations. The reported experiments were executed with co-current NBI injection. To avoid for the poorly understood influence of detachment on the ELM power loading either due to an increased energy transport caused by local divertor plasma [8] or buffering of ELMs by radiation [12], data for ASDEX Upgrade are used with both divertor legs (in both field directions) not being power detached. For JET only forward field data in LSN are used due to diagnostical restrictions. Also it must be noted that for JET literally no case is within the data base of IR suitable discharges without the inner leg being (partly) power detached. Experimental details of the magnetic configurations, discharge parameters and diagnostic can be found in [11] for ASDEX Upgrade and in [6] for JET. All data presented are based on conditional ELM averaging of about 15–30 ELMs.

2. Description of the temporal evolution of ELM power loading

A single particle expression was introduced to describe the power deposition at the divertor target plates in the limit of entirely force free convective transport of particles along open field lines in the SOL. In this approximation (see Eqs. (4.1)–(4.10) in [1] for details) the temporal evolution of arrival of particles and energy at the divertor target plates is due to free-streaming of a Maxwellian distribution (e.g. ions with temperature T_i) released on a short time, $\delta(t)$, and parallel distribution length, $\delta(s)$, when compared to the parallel transport times and parallel connection lengths to the target. In the latter contribution, the Maxwellian distribution was characterised by a zero mean velocity and by default the energy load due to ELMs on the inboard and outboard divertor targets are identical (energy out/in ratio 1:1). The actual observed ELM power load asymmetry cannot be described if the Maxwellian mean velocity is set to zero.

In this contribution we extend the model [1] by allowing for non-zero mean velocities. As it is known that the plasma rotates toroidally [13], we assume the pre-ELM pedestal rotation of the particles to set the parallel velocity of the particles, released during an ELM, and expressed in terms of the pedestal Mach number. For simplicity in the discussion we assume the poloidal rotation to be zero and the radial electric field in the SOL to vanish. As convention, a positive Mach number describes toroidal rotation in co-current direction. The latter quantity is called $M_\parallel = v_{tor}/c_s$, where $c_s = \sqrt{(T_e + T_i)/m_D}$ is estimated with the pedestal top electron temperature prior to the ELM event ($T_i = T_e = T_{ped}^{measured}$). The quantity v_{tor} describes the toroidal plasma rotation and details on measurements can be found in [13]. This extended approach, which we will call for convence free-streaming-particle (FSP) approach is derived by estimating the arrival time of each particle of the Maxwellian distribution at the target plate in a distance $L_\parallel^{ELM}$ from the particle origin. The particle rate, $\Gamma(t)$, arising from an arbitrarily defined distribution, $f_v(v)$, of particle velocities (in one dimension, here the direction along field lines) is given [1] by

$$\Gamma(t) = f_v(v) \times \frac{dv_{target}}{dt} \quad \text{with } v_{target} = \frac{L_\parallel^{ELM}}{t}. \tag{1}$$

By inserting a Maxwellian distribution for $f_v(v)$ and using N_{ELM} for the overall number of target deposited particles, the particle rate at the (divertor) target is given by

$$\Gamma(t) = \frac{N_{ELM}}{\sqrt{\pi} c_s} \times \exp\left(-\left(\frac{v_{target} - v_0}{c_s}\right)^2\right) \times \frac{-L_\parallel^{ELM}}{t^2}. \tag{2}$$

Using $v_{target} = L_\parallel^{ELM}/t$, $\tau_{FSP}^{o,i} = L_\parallel^{o,i}/c_s$ and identifying all particles with positive parallel velocities as those hitting the outer divertor ($L_\parallel^{ELM} = L_\parallel^{o}$), those with negative parallel velocities streaming to the inner divertor target ($L_\parallel^{ELM} = -L_\parallel^{i}$), we get

$$\Gamma_{o,i}^{ELM}(t) = \frac{N_{ELM}}{\sqrt{\pi}} \times \exp\left(-\left(\frac{\tau_{FSP}^{o,i}}{t} - H_{fl}^{o,i} M_\parallel\right)^2\right) \times \frac{\tau_{FSP}^{o,i}}{t^2} \tag{3}$$

with $H_{fl}^{o,i}$ giving the orientation of the field line helicity in respect to the inboard and outboard targets. By using two parameters for the magnetic configuration and divertor geometry, $G_{LSN}^{USN} = 1$ for LSN discharges, $G_{LSN}^{USN} = -1$ for USN discharges, $D_{target}^{i} = +1$ for the inner target and $D_{target}^{o} = -1$ for the outer target the following convention is used:

$$H_{fl}^{o,i} = sign(B_{tor}) \times sign(I_p) \times G_{LSN}^{USN} \times D_{target}^{o,i}. \tag{4}$$

A positive Mach number, $M_\parallel > 0$ will drive more particles to the inner target for $-B_{tor}/+I_p$ in LSN and for $+B_{tor}/+I_p$ in USN discharges. For $-B_{tor}/+I_p$ in USN and identical Mach number the exactly inversed asymmetry is predicted. It should be noted that the only difference for the expression of the inner, $\Gamma_i(t)$, and the outer, $\Gamma_o(t)$, target particle rates are the values for $L_\parallel^{o,i}$ and $H_{fl}^{o,i}$.

Finally, we express the divertor power $p_{o,i}^{ELM}$ normalised to the overall ELM target deposition energy $E_o + E_i$. Following the analysis in [1] the average energy of a target deposited particle is equal to $kT_\perp + m_D v^2/2$ where $T_\perp$ describes the perpendicular particle energy which is not affected by parallel losses resulting in

$$p_{o,i}^{ELM}(t) = \frac{2}{3}\frac{E_o + E_i}{\sqrt{\pi}} \times \left(1 + \left(\frac{\tau_{FSP}^{o,i}}{t}\right)^2\right) \times \frac{\tau_{FSP}^{o,i}}{t^2} \times \exp\left(-\left(\frac{\tau_{FSP}^{o,i}}{t} - H_{fl}^{o,i} M_\parallel\right)^2\right). \tag{5}$$

3. Numerical fitting to experimental data

Fig. 1 presents a comparison of experimental data taken in ASDEX Upgrade upper single null discharges (see [6,11]) estimated by IR thermography to numerical fitting of Eq. (5) with a least square method. The reader should note that beside setting the inter-ELM power flux value and absolute time of the ELM onset, only four fitting parameters are used for both, the inner and outer ELM power load evolution, simultaneously. These are the ELM target energy for both targets ($E_o + E_i$), the Mach number, $M_\parallel$ and the time scales τ_{FSP}^{o} and τ_{FSP}^{i}.

The agreement of experimental data to the numerical fit of Eq. (5) appears to be reasonably well as shown in Fig. 1. Various details should be noted. First, for both discharges in Fig. 1 with similar pedestal plasma parameters and identical NBI heating and q_{95} literally identical time scales are found. Secondly, typically $\tau_{FSP}^{i} \approx 1.1 \times \tau_{FSP}^{o}$ is found. Finally, the in/out asymmetry of the time integrated ELM energy load in both field directions can be explained by the introduction of a Mach number in the Maxwellian velocity distribution of released particles. For the presented case the absolute value is around $M_\parallel \approx 0.1$. As mentioned, the origin of the parallel Mach number is assumed to arise from the toroidal pedestal rotation. Given typical values for $\tan\alpha = B_{pol}/B_{tor} \approx 0.1$ with B_{pol} being the local poloidal magnetic field in the pedestal region, and further assuming a mainly toroidal pedestal rotation $M_\parallel = M_{ped} \times \cos\alpha$, it follows that $M_\parallel \approx M_{ped}$. The measured toroidal pedestal rotation by edge CXRS for similar discharges in ASDEX Upgrade M_{ped} is found to be around 15–30 km/s in co-current direction in the pedestal top region. An electron temperature at the pedestal top $T_{ped} \approx 600$ eV is found. Given the pedestal Mach num-

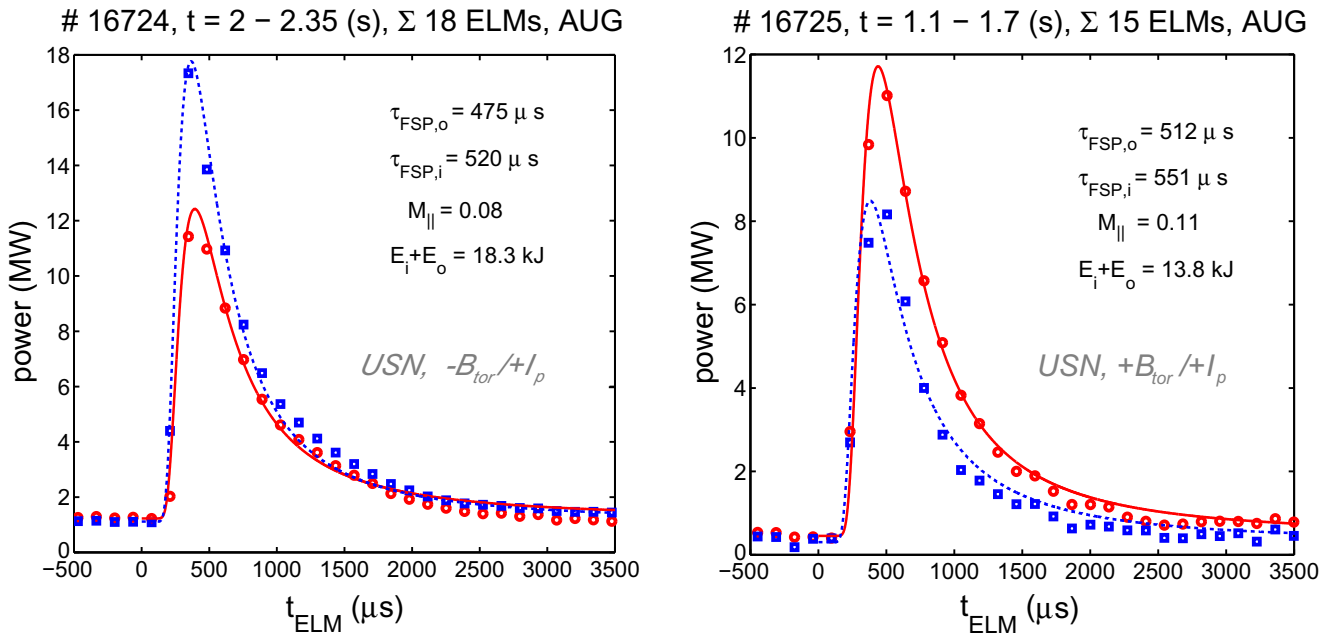

Fig. 1. Experimental data of ELM power deposition (inner target red circles, outer target blue squares) and numerical fit (inner solid red line, outer dashed blue line) of $p_{o,i}^{ELM}(t)$ for type-I ELMy H-mode in USN in ASDEX Upgrade with (left) $B_{tor} = -2.0\,\mathrm{T}/I_p = +0.8$ MA and (right) $B_{tor} = +2.0\,\mathrm{T}/I_p = +0.8$ MA. (For interpretation of the references in color in this figure legend, the reader is referred to the web version of this article.)

ber $M_{ped} \approx 0.1$ and $c_s \approx 238$ km/s we find reasonable agreement with the CXRS measurements. Unfortunately, simultaneous measurements of the edge toroidal and poloidal pedestal rotation and the ELM in/out power load asymmetries are currently not available but foreseen for future studies.

Fig. 2 presents data taken for a JET discharge in IR optimised magnetic configuration [6]. Due to diagnostic imperfections the data quality when compared to ASDEX Upgrade is comparable weak and in particular the inboard target power load is difficult to measure on the appropriate time scales required for the analysis here [14]. However, the result of data fitting shows still fair agreement. For the inner target not a numerical fit but a best guess is shown. Comparison to typical pedestal rotation values for JET from CXRS also finds reasonable agreement.

4. Comparison of empirical values for $E_{\tau_{IR}}$ and the FSP approach

In absence of a detailed understanding of the ELM parallel transport so far empirical studies have been used for the assessment of ELM divertor power for ITER [5,10,15,16]. We do not attempt to discuss this issue here completely but focus on an important implication arising from the latter findings, namely the energy fraction in the rise phase, $E_{\tau_{IR}}$ [5,15] defined as

$$E_{\tau_{IR}}^{o,i} = \frac{\int_0^{\tau_{IR}} p_{o,i}^{ELM}(t)dt}{\int_0^{\infty} p_{o,i}^{ELM}(t)dt}. \quad (6)$$

From Eq. (5) τ_{IR} can exactly be estimated by setting

$$p_{o,i}(\tau_{IR}) = p_{o,i}^{max}, \quad (7)$$

$$\rightarrow \tau_{IR} = 0.39 \times \tau_{FSP}^{o,i}. \quad (8)$$

Inserting $\tau_{IR} = 0.39\tau_{FSP}$ into Eq. (6), it follows $E_{\tau_{IR}} = 18\%$ and is found to be independent of the value of τ_{FSP} and only little depending on the value for $M_{||}$. The energy fraction leading to the maximum *temperature* excursion on the divertor target surface, $E_{\tau_{IR}}^{T_{max}}$, depends on the values for the heat conduction, heat capacity and material density as well as the absolute target surface temperature values. For typical inter-ELM target temperature of around 1000 °C and CFC (or W) targets the maximum temperature peaks about 50–100 μs later in time than the maximum power, which is just below the temporal resolution of the IR camera systems and this way coincides with the experimental error bars for estimating $E_{\tau_{IR}}$. The typical value for $E_{\tau_{IR}}$ when related to the maximum temperature excursion, $T_{target}(\tau_{IR}^{CFC}) = T_{target}^{max}$, for CFC is found to be around $E_{\tau_{IR}}^{T_{max}} = 25\%$. Fig. 3 presents the values experimentally observed for outer target in JET IR optimised discharges which compares well with the prediction by the FSP approach.

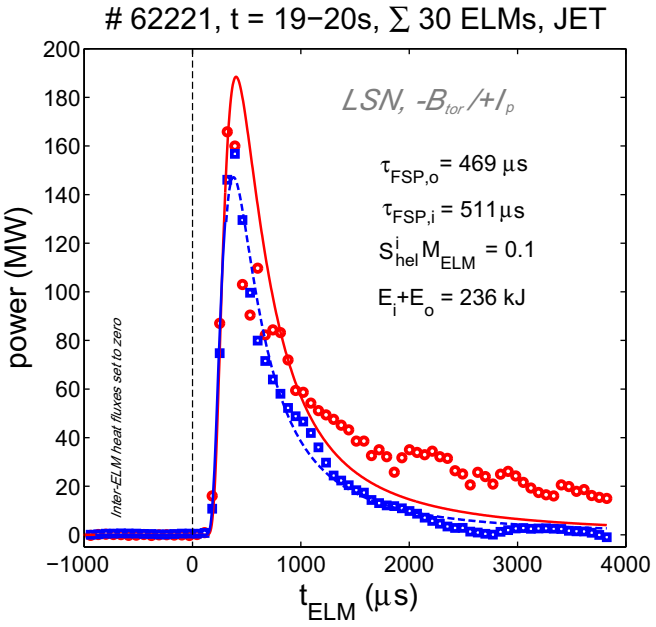

Fig. 2. Comparison of FSP approach to ELM power load for a JET IR optimised magnetic configuration with $B_{tor} = -3.0\,\mathrm{T}/I_p = 3.0$ MA. Same color and marker index as Fig. 1. (For interpretation of the references in color in this figure legend, the reader is referred to the web version of this article.)

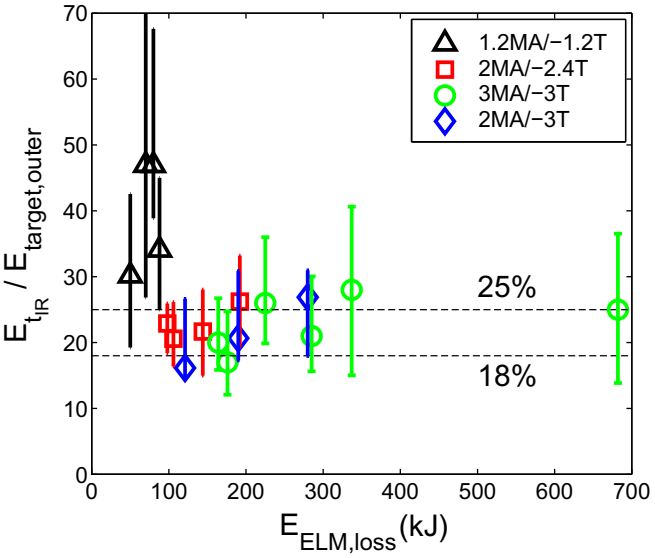

Fig. 3. Comparison of $E_{\tau_{IR}}$ (see text) for the outer divertor given by the FSP approach to data taken from 17 discharges in IR optimised configuration with different ELM sizes and plasma currents with $-B_{tor}/+I_p$ (forward) field.

5. Discussion

A comparable simple analytical model is able to reproduce the ELM inboard/outboard power load time scales and integral energy values. In the approach basically only ion transport time scales are considered and faster energy transport due to electrons is ignored. The approach is found to work well for cases with both divertor legs not being power detached between and during ELMs. Though various aspects cannot be described self-consistently, i.e. the required charge separation is not explained, the good match between experimental data and the FSP model points on the importance of taking into account the pedestal rotation for the transient heat loads caused by ELMs. To reproduce the ELM in/out power load asymmetries reasonable numbers for the pedestal Mach number are derived. Additionally, the explanation of the observed change of the in/out asymmetry with field line helicity by changing the B_{tor} direction is a further important feature of the approach. It should be noted that this approach does not require any effects due to drifts. However, only combined measurements of the pedestal Mach number and power load characteristics for any combination of $\pm B_{tor}$ and $\pm I_p$ or co/counter NBI are able to give further insight or evidence.

Studies using the kinetic modelling [17] report that more than 95% of the ELM deposited energy arrives at the target plates with the typical time scale of $\tau_{\|} = L_{\|}^{ELM}/c_s$, hence in agreement to the basic assumption of convectively (ion) dominated energy transport in the FSP approach. However, it must be noted that the found numerical values for τ_{FSP} do not match a simple geometrical interpretation where the ELM energy release location is the outer midplane and connected by about $L_{\|}^{o} = 1/3 \times 2\pi q_{95} R$ to the outer target and by $L_{\|}^{i} = 2/3 \times 2\pi q_{95} R$ to the inner target. For ASDEX Upgrade by using $T_{ped} \approx 600$ eV, $q_{95} = 4.3$ and $R = 2.1$ m values for $\tau_{FSP}^{o} = 80$ μs and $\tau_{FSP}^{i} = 160$ μs are found. For JET $T_{ped} \approx 1200$ eV, $q_{95} = 3.3$ and $R = 3.8$ m is used giving values of $\tau_{FSP}^{o} = 78$ μs and $\tau_{FSP}^{i} = 156$ μs, hence much shorter than the real observed numbers. Also, $\tau_{FSP}^{i} \approx 2\tau_{FSP}^{o}$ should be found which is not the case. Possible ways to explain the difference to the actual numbers for τ_{FSP} when compared to $L_{ELM} = 2\pi q_{95} R$ are given by taking into account an ELM energy release time of about τ_{IR} itself. For the instance given here 275 μs are required for the ELM energy release time to explain the difference. This number is estimated by numerical convolution of Eq. (5) with an ELM energy release function. Complementary, an effective connection length during ELMs ($L_{\|}^{o,i}$) significantly larger than $L_{ELM} = 2\pi q_{95} R$ caused by ergodization or reconnection [18] is able to resolve the discrepancy. Since both latter numbers will give insight into the ELM instability mechanism, further efforts to resolve the observed timescales are mandatory for future studies. Also it has to be noted that the resolution of the used IR diagnostical systems of about 136 μs for ASDEX Upgrade and 97 μs for JET in combination with conditional ELM averaging may cause some temporal smearing of the data, which can only be overcome by improved diagnostics.

Various other aspects are worth notifying in that respect. The inboard/outboard power load asymmetry is strictly dependent in the FSP approach on the projection of the pedestal rotation onto the SOL field lines. For plasmas toroidally rotating in counter-current direction the in/out balance is predicted to deposit more power to the outer target for $-B_{tor}/+I_p$ (*normal*) field direction in LSN configuration. Such results were recently presented from JT-60U ELM divertor target power analysis [19] and are fully consistent to the proposed new picture here. It also may be worth mentioning that the FSP approach only applies for convective ELMs. Mainly convective ELMs are observed usually at high densities and small ELM amplitudes. Small convective ELMs in DIII-D are reported to be more asymmetric than larger ELMs which show a higher fraction of conductive losses [8,20]. Following the analysis here, the in/out asymmetry for small convective ELMs would be influenced more by the pedestal rotation than conductive ELMs, qualitatively consistent with the results presented for DIII-D [8].

In summary we conclude that the good agreement between the analytical description and the measured data of the target power implies that the plasma rotation has to be included for any complete description of ELM divertor heat loads. Also, the reported differences from the various tokamak devices about the ELM in/out energy load asymmetry may be caused by the quite different heating scenarios and resulting details for plasma rotation with co- and counter neutral beam injection, and further effects caused by ripple and direct orbit losses.

References

[1] W. Fundamenski, R.A. Pitts, Plasma Phys. Control. Fus. 48 (2006) 109.
[2] A. Leonard et al., J. Nucl. Mater. 241–243 (1997) 628.
[3] A. Loarte et al., Plasma Phys. Control. Fus. 45 (2003) 1549.
[4] A. Loarte et al., Phys. Plasma 11 (2004) 2668.
[5] T. Eich et al., J. Nucl. Mater. 337–339 (2005) 669.
[6] T. Eich et al., J. Nucl. Mater. 363–365 (2007) 989.
[7] A. Kallenbach et al., Nucl. Fus. 48 (2008) 085008.
[8] M. Fenstermacher et al., Plasma Phys. Control. Fus. 45 (2003) 1597.
[9] S.H. Hahn et al., Phys. Plasma 12 (2005) 102501.
[10] D.N. Hill et al., J. Nucl. Mater. 241–243 (1997) 182.
[11] T. Eich et al., Plasma Phys. Control. Fus. 47 (2005) 815.
[12] A. Loarte et al., in: Proceedings of the IAEA Fusion Energy Conference, Sorrento, Italy, 2000.
[13] P. de Vries et al., Nucl. Fus. 48 (2008) 065006.
[14] T. Eich et al., Plasma Phys. Control. Fus. 49 (2007) 573.
[15] A. Loarte et al., J. Nucl. Mater. 313–316 (2003) 962.
[16] A. Leonard et al., J. Nucl. Mater. 266–269 (1999) 109.
[17] D. Tskhakaya et al., J. Nucl. Mater. 390–391 (2009) 335.
[18] T. Evans et al., J. Nucl. Mater., accepted for publication.
[19] A. Takizuka et al., Control. Plasma Phys. 48 (2008) 207.
[20] A.W. Leonard et al., Plasma Phys. Control. Fus. 45 (2003) 1597.